Computational study of transient flow around Darrieus type Cross Flow Water Turbines

O. López[1], D. Meneses[1], B. Quintero[2] and S. Laín[*2]

[1]*Computational Mechanics Research Group. Department of Mechanical Engineering, Universidad de los Andes,111711 Bogotá, Colombia*
[2]*Fluid Mechanics Research Group. Department of Energetics and Mechanics, Universidad Autónoma de Occidente, 760030 Cali, Colombia*

Abstract: This study presents full transient numerical simulations of a cross-flow vertical-axis marine current turbine (straight-bladed Darrieus type) with particular emphasis on the analysis of hydrodynamic characteristics. Turbine design and performance is studied using a time-accurate Reynolds-averaged Navier–Stokes (RANS) commercial solver. A physical transient rotor-stator model with a sliding mesh technique is used to capture changes in flow field at a particular time step. A shear stress transport k-ω turbulence model was initially employed to model turbulent features of the flow. Two dimensional simulations are used to parametrically study the influence of selected geometrical parameters of the airfoil (camber, thickness and symmetry-asymmetry) on the performance prediction (torque and force coefficients) of the turbine. As a result, torque increases with blade thickness-to-chord ratio up to 15% and camber reduces the average load in the turbine shaft. Additionally, the influence of blockage ratio, profile trailing edge geometry and selected turbulence models on the turbine performance prediction is investigated.
Key words: Cross flow water turbine, unsteady CFD flow simulation, turbulence model.

1 Introduction

Exhaustion of fossil fuels resources combined with greenhouse gas negative impact has raised the interest for renewable energies since a few decades ago. Among them, hydropower takes a particular place because of its huge potential. In the last years, tidal power based on tidal currents has become very attractive because of its high energy density, high predictability and low environmental impacts. The estimated tidal energy potential worldwide reaches around 600 TWh/yr [1] (cited by [2]), from which around 120 could be harvested, and it is being largely underused. Also, following the International Renewable Energy Agency in its report of 2014 [3], the technically harvestable tidal energy resource from those areas close to the coast, is estimated at 1 terawatt (TW).

Tidal current turbines shapes are inspired from wind turbine shapes and they can be classified depending on the direction of the rotational axis relative to the water flow direction. Axial flow water turbines (AFWT) have their axis of rotation parallel to water stream direction. Other turbines, cross flow water turbines (CFWT) or Darrieus type water turbines, have rotational axis perpendicular to current direction. A vertical-axis turbine has smaller efficiency than AFWT but is able to extract power from any direction of the main

[*]Corresponding author. Phone +57 2 3188000 Ext. 11882, e-mail: santiago.lain@gmail.com

stream without adjustment. A Darrieus turbine is a fixed pitch CFWT with straight blades, directly connected to the shaft by struts, and its simplicity lies in the absence of the orientation and yawing mechanisms. This type of turbine is particularly promising for being used to extract energy from tidal currents due to its relatively simple design and easiness of manufacturing which are translated in lower production costs. Additionally, recent studies [4-5] show that CFWT can be installed much closer than AFWT, so that the power density per square meter can be considerably high. Nevertheless, the aerodynamics of the Darrieus turbine is far from being simple since it involves highly unsteady flow fields. This unsteadiness is due to large variations in the angle of attack on the blades during their rotation.

Design, development and optimization of tidal turbines require accurate and time-efficient mathematical models. Based on the computational tools available, different models with different computational costs were developed and applied for optimization and analysis purposes. These models range from momentum models, vortex models, to three-dimensional computational fluid dynamics (CFD) models of turbine with all the physical details taken into account. Momentum models such as single or multiple stream tube model are computationally inexpensive but cannot predict the structure of the wake. Vortex models based on potential flow have better predictions of the power output but are computationally more expensive than momentum models and some details of the structure of the wake are missed if flow separation at the leading edge of the blades is not included in the model. On the other hand, vortex methods need to include lift and drag experimental information for computing forces and torques on the blades; moreover, the effects of shaft and supporting arms must be obtained by experimental field data. With the use of powerful computers and parallel processing technology, CFD simulations are becoming more popular in industrial and academic sectors [6 – 9]. Contrary to potential flow codes, CFD simulations do not need any external data (experimental lift and drag) and can include separation from foils and drag induced vortices from turbine's shaft. Also, they are able to simulate dynamic stall phenomenon (although it is not perfect due to the limitations of turbulence models). CFD modelling is also a powerful tool for complex geometries.

The main advantage of CFD is that it allows reproducing physical unsteady flow around turbine using the so-called sliding mesh methodology, wherein relative motion between steady domain and rotor (unsteady domain) is captured by coupling them through an interface, which is updated at each time step and allows conservative interchange of fluxes between both domains. The rotor grid turns at each time step an angle relative to the steady domain. At each time step a new solution is calculated. Transient behavior is built by adding solutions at each time step. In this methodology, integral values (torque) must be averaged in a complete revolution. The main disadvantage of CFD simulations for tidal turbines, regarding potential flow methods (momentum and vortex models), is its higher computational cost (CPU time and memory). This is the reason why there are not many publications applying this methodology to CFWT.

Compared with horizontal axis turbines, there are not many previous studies approaching the simulation of vertical axis machines, considering water as fluid, from the same perspective as suggested here. Ferreira [10], employing air as fluid, presented a detailed state of art of different strategies for predicting aerodynamic characteristics of a VAWT. This author performs an exhaustive study about the ability of different turbulence models

(Spalart-Allmaras, k-ε, Detached Eddy Simulation, DES, and Large Eddy Simulation, LES) to reproduce the dynamics of the detached vortices from a single airfoil in two dimensions during its trajectory in the half cycle upstream of a VAWT. The best comparisons with experiments are obtained for LES, but the computational cost is prohibitive to think about useful design and evaluations from a practical point of view. This fact is common when LES is applied to industrial relevant flows.

Also using air as fluid, Maître *et al* [11] applied the sliding mesh strategy to a two bladed VAWT using Fluent v. 6.0 software combined with the one equation turbulence model Spalart-Allmaras. These authors defined two zones, an outer fixed zone and another inner rotating zone containing the blades. The results were compared with experimental data [12], obtaining an overprediction for the measured aerodynamic forces on the airfoils. However, in this paper no geometric details of the considered turbine were given.

Howell et al. (2010) [13] developed a combined experimental and computational study of the aerodynamics and performance of a small (aspect ratio of 4) vertical axis wind turbine straight-bladed Darrieus type with three blades. Two- as well as three-dimensional numerical simulations were performed using the commercial code Fluent in connection with the k-ε RNG turbulence model. Authors found that the power coefficient of the two-dimensional computations was significantly higher than that of the three-dimensional calculations and the experimental measurements, which was attributed to the presence of the over tip vortices in the three-dimensional situation.

Using water as fluid, Nabavi [14] performed a two-dimensional very detailed numerical study about hydrodynamic performance of a three-bladed CFWT introduced in a duct, to accelerate flow upstream the turbine. The author compared the two dimensional computational results obtained with Fluent in free flow conditions with own experimental measurements, resulting in an overprediction of the power coefficient. This result is in line with that obtained by Maître *et al* [11] because both used the Spalart-Allmaras turbulence model. Additionally, Nabavi (2008) [14] tried other RANS models (k-ε, k-ω and Reynolds Stress model) obtaining similar qualitative results. However, based on the results discussed in section 8, the present authors believe that the use of the Spalart-Allmaras turbulence model in these specific simulations cannot be recommended in general because of its poor performance, even with the curvature correction included, and its computational cost which is as high as a two-equation turbulence model.

Dai & Lam [15] also performed a two-dimensional numerical study of three-bladed CFWT using the software ANSYS CFX v. 11, which is extensively employed for numerical simulation of hydraulic turbomachines. In this case, the turbulence model chosen was the two equation model SST (Shear Stress Transport). As in [14], they validate their numerical results versus own experimental measurements performed in a towing tank. The quantitative results of the validation are, however, only provided in a point, comparing them with the experiments and also with the results obtained by the double multiple streamtube model. As in the former studies, the averaged values of the torque provided by CFD are above the experimental values. In this study, enough information was provided about geometric parameters of turbine, so this configuration has been chosen in the present work.

Amet et al. (2009) [16] performed a very detailed 2D simulation of two-bladed CFWT and compared with experimental data of several authors [12,17,18] for two tip speed ratios (TSR) of 2 and 7. In this paper a very refined structured grid is used around the airfoils with a value of y^+ around 1. The authors also comment that "Due to some numerical instabilities at the trailing edge, the sharp edge was transformed into a round edge with a ratio radius/chord of 0.1%. The results are not affected by this tiny transformation". An extensive discussion about the blade-vortex interaction is developed in this paper concluding that the flow in the case of the smaller tip speed ratio was characterized by a deep stall regime with several large vortices detached from the blades while for the higher TSR the flow is characterized by a weak shedding of alternated vortices in the upstream half disk and by an attached flow in the downstream half disk.

Li and Calisal (2010) [19] studied the three-dimensional effects in a vertical axis tidal turbine with a vortex model especially developed of this purpose. Computational results that were corrected for arm effects, show very good agreement with experimental results obtained in a towing tank. It was concluded that three-dimensional effects are significant when the turbine height is less than two times the turbine radius. If the turbine height is at least six times the turbine radius then the three-dimensional effects are negligible.

Coiro et al. [6,20] implemented the Double Multiple Streamtube model for the simulation of two models of straight-bladed turbines, including one called the "Kobold" prototype which is actually installed in the Strait of Messina, Italy. Numerical results of the evolution of the power output of the turbine is in very good agreement with experimental data measured in both wind-tunnel and field data measured for the Kobold prototype. Dynamic effects had to be included in the model in order to correctly predict the power output of the Kobold prototype.

Maître et al. (2013) [21] simulated in two dimensions with great detail the three bladed model CFWT LEGI available in their laboratory. The paper discusses the dependence of the results on the grid refinement close to the blade surface, focusing in the mean power extracted. The main conclusions obtained by the authors were: 1. The obtained mean power decreases fast when the grid coarsens in the proximity of the profiles surface, 2. A coarse mesh induces an early and severe loss of lift due to the formation of a back flow bubble, which generates unrealistic pressure drag. Moreover, in the same line as found by other authors, the predicted power coefficient is notably higher than the experimental values, except for very low tip speed ratios where computations are below the measurements. This work also cites the three-dimensional simulations of Amet (2009) [22] on the same water turbine performed for just one tip speed ratio employing a grid with 8 million nodes. In such a case the computed power coefficient was very close to the measured value in best efficiency point. In this last study also it is mentioned that the influence of the detached tip blade trailing vortices on the turbine performance loss is around 22%.

Very recently, Jin et al [23] review the different methods (both numerical and experimental) currently used to study Darrieus type vertical axis wind turbines (VAWT's). Regarding the CFD models, these authors stress that two dimensional simulations are still widely used to improve efficiency, to evaluate the effects of meshing on computational results and to evaluate the effect of turbulence modelling on computational results. In comparison with 3D CFD models, 2D CFD models are considered simpler to implement and faster to compute but 3D models provide higher numerical precision. However, the CPU cost of the 3D computations is much higher, around 100 times more than the 2D. In this respect, Song et al. [24] performed 2D simulations to investigate the influence of various meshing strategies and turbulence models on the prediction of performance of VAWT's.

Lanzafame et al [25] performed 2D simulations of a 3-bladed Darriues type turbine, using ANSYS-Fluent. The main objective of this study was to demonstrate the capabilities of transitional turbulence models in the prediction of the turbine performance. It was found that using fully turbulent RANS model in general overestimated of the power coefficient, but transitional models showed better agreement with experimental data. 3D simulations are considered for future research using transitional turbulence model due to computational cost. Chen and Lian [26] performed 2D simulations in ANSYS-Fluent to study the vortex dynamics of a Darrieus wind turbine using the k-epsilon model and meshes with y^+ greater than 15. It was found that the vortex-blade interaction depends on the solidity and the tip speed ratio. The influence of the thickness of symmetric airfoils on the torque coefficient was also studied. Trivellato and Castelli [27] also performed 2D simulations of a Darrieus type turbine in order to study the Courant-Friedrichs-Lewy criterion when using sliding mesh technique in ANSYS-Fluent. It was concluded that a CFL criterion smaller than 0.15 appears to be adequate but this implies a dramatic increase in CPU time. Guidance to correctly choose meaningful angular marching steps of rotating grids is provided. Paillard et al [28] performed 2D CFD simulations of a cross flow tidal turbine with ANSYS-CFX including sinusoidal pitch control. It was found that a 52% improvement in the tangential force could be achieved when the second harmonics was used in the pitch control. Simulations were run fully turbulent but the authors believed that a transitional turbulence model is necessary in this type of simulations.

The present study performs full transient simulations of flow around a straight bladed CFWT using CFD tools, including underlying turbulence of fluid flow and also viscous effects, without employing tabulated lift and drag data. This reason has motivated the choice of the sliding mesh method, which is the only one that allows describing the real unsteady behaviour of the CFWT blades in the fluid domain. After introduction, section 2 resumes the vertical axis turbine operation parameters. Sections 3, 4 and 5 describe the geometry and meshing procedure of the turbine, the numerical simulation methodology and the results of the verification and validation study, respectively. Section 6 presents the sensitivity of results to the employed turbulence model. In section 7, two dimensional simulations are used to study the influence of selected geometrical parameters of the airfoil on the performance prediction (torque, tangential force and normal force coefficients) of the turbine. The airfoil thickness and symmetry were the selected factors for the present parametric study. The vortex-blade interaction along a complete revolution is also discussed. Additionally, the influence of blockage ratio and the shape of the profiles trailing edge on the turbine performance prediction is briefly discussed in sections 8 and 9. Section 10 compares the two-dimensional torque coefficient predictions with preliminary three-dimensional results; moreover, the 3D simulation allowed visualising the tip blade trailing vortices as well as the shape of the bound vortex. Finally, conclusions are drawn in the last section.

2 Vertical axis turbine operation

Hydraulic operation of a cross flow water turbine can be characterized by rotor torque M, rotor drag D, rotor angular velocity ω and power output P = ω M. The main dimensionless parameters are the following:

Tip speed ratio (TSR), $\lambda = \omega R / V_0$ (1)

Torque coefficient, $C_m = M / \left(\frac{1}{2} \rho V_0^2 R S_{ref} \right)$ (2)

Power coefficient or efficiency, $C_P = P / \left(\frac{1}{2} \rho V_0^3 S_{ref} \right)$ (3)

Drag coefficient, $C_D = D / \left(\frac{1}{2} \rho V_0^2 S_{ref} \right)$ (4)

Here, R represents the radius of rotor, V_0 the incident current velocity, ρ the water density and S_{ref} the cross section ($S_{ref} = 2RH$ for CFWT). Solidity is defined as $\sigma = NC/R$ with N the number of blades and C the chord length. Finally, H is the blade span.

Turbine blades rotate around vertical axis with rotational velocity $\vec{\omega}$. In 2D cylindrical coordinates (r, θ), the blade local relative velocity $\vec{W}$ corresponding to an incident flow velocity $\vec{V}_0$, is given as:

$$\vec{W} = \vec{V}_0 - \vec{\omega} \times \vec{R} \quad (5)$$

When a blade rotates, its angle of attack α (the angle between local relative velocity and chord) changes leading to variable hydrodynamic forces as (see Fig. 1):

$$\alpha = \tan^{-1}\left(\frac{\sin\theta}{\lambda + \cos\theta} \right) \quad (6)$$

where θ is the counterclockwise rotation angle of the airfoil along the circumference. θ = 0º is taken from the upper point of the circumference where the profile is aligned with the incoming flow.

Resultant hydrodynamic force acting on the blades is decomposed in two components (normal F_n, perpendicular to chord; and tangential F_t, parallel to chord). Forces values can be inferred from classical computations over an airfoil in an unbounded domain or from available experiments in wind tunnel tests at fixed α and Reynolds number. The tangential force coefficient is the dimensionless form of F_t and it is directly related to the turbine torque. Negative tangential component is responsible for turbine rotation. In the upstream semicircle, with θ increasing from 0º position, tangential force becomes negative and reaches a minimum near θ = 90º before increasing until θ = 180º. The same behaviour occurs in downstream semicircle between θ = 180º and 360º positions. In vicinity of θ = 0º and 180º positions, the blade has a positive tangential component force F_t, opposed to rotational motion. In this configuration of blades, small tip speed ratios lead to large incidence variations during a revolution. In particular, α becomes very large and overtakes the static stall angle of airfoils, about 12-15º. The normal force coefficient is the dimensionless form of F_n, so is related to cycle loading and fatigue on the turbine shaft. Since the simulations are performed in a $X-Y$ reference frame, forces coefficients (C_x and C_y) are numerically obtained in this system (see Fig. 1). A simple transformation (rotation) is needed between the $X-Y$ coordinate system and the tangential – normal $t-n$ system of the airfoil (see Eq. 7).

$$\begin{aligned} C_t &= C_{tx} + C_{ty} = C_x \cos(\theta) + C_y \sin(\theta) \\ C_n &= C_{ny} - C_{nx} = C_y \cos(\theta) - C_x \sin(\theta) \end{aligned} \tag{7}$$

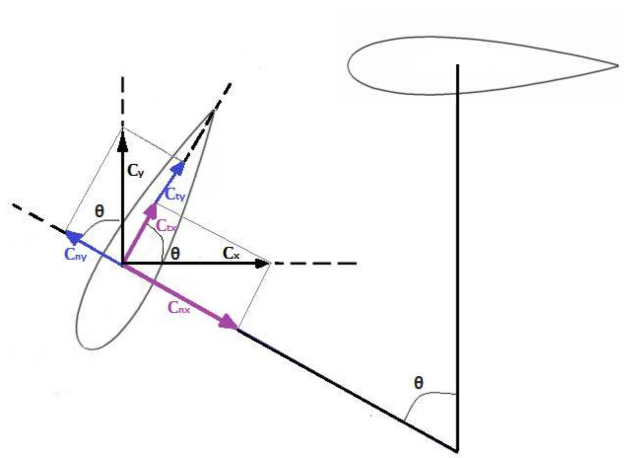

Fig. 1. Coordinate system defining the force coefficients of the profile.

Nevertheless, real flows around blades in CFWT differ from above conclusions because of two reasons: i) Relative flow passing through a CFWT blade is unsteady; and ii) Oncoming far field seen by a blade is not V_0, but some unspecified velocity. Moreover, the flow field around a Darrieus type CFWT is inherently unsteady and three-dimensional due to the dynamic stall phenomenon experienced by a rotating blade and also to the interference of detached vortices from moving blades [12, 17]. Such vortices tend to stay near the generating blade. As a result of the strong coupling between them and the flow around the blade lift increases, improving turbine efficiency. However, although the presence of dynamic stall at low tip speed ratios can have a positive impact on the power generation of the turbine, the formation of vortices can generate other problems such as vibrations, noise and reduction of fatigue life of the blades due to unsteady forces. Larsen et al. (2007) [29] show that dynamic stall is mainly characterized by flow separations at the suction side of the airfoil. This can be summarized in four crucial stages: 1) Leading edge separation starts, 2) Vortex build-up at the leading edge, 3) Detachment of the vortex from leading edge and build-up of trailing edge vortex, 4) Detachment of trailing edge vortex and breakdown of leading edge vortex. The sequence of these four flow events will generate unsteady lift, drag and pitching moment coefficients with a large range of flow hysteresis dependent on the angle of attack [30].

3 Geometrical configuration and mesh generation

The CFWT studied in Dai & Lam (2009) [15] has been chosen in this work due to availability of all geometric data (Diameter D = 900 mm, H = 700 mm; reference area S_{ref} = 0.63 m^2) of the turbine. The straight blades are based on the symmetric NACA0025 airfoil. The considered case has been 3S2R1 [15] (profile chord, C = 132.75 mm), resulting in a solidity σ = 0.89. The turbine rotates with a constant angular velocity of 6.28 rad/s

As it was mentioned in the introduction, the geometry employed in the simulation was a two-dimensional version of the real three-dimensional turbine. Moreover, neither the supporting arms of the blades nor the shaft have been included as in reference [15]. The dimensions of the two-dimensional simulation domain were eight rotor diameters in length and five rotor diameters in width, resulting in a blockage ratio of 20% [14].

The boundary conditions employed in the two-dimensional computations consist of a velocity inlet on the left side, a pressure outlet on the right side and two moving walls on top and bottom with the same fluid velocity as the inlet. Moreover, the profiles representing the blades are in the inner part of a rotating ring, which is separated from two steady domains, inner and outer, by two sliding interfaces specified as a boundary condition of type sliding mesh. Finally, as the inflow turbulence conditions are not known, a turbulence intensity of 10% has been assumed at the inlet. A sketch of the computational domain and boundary conditions is shown in Fig. 2.

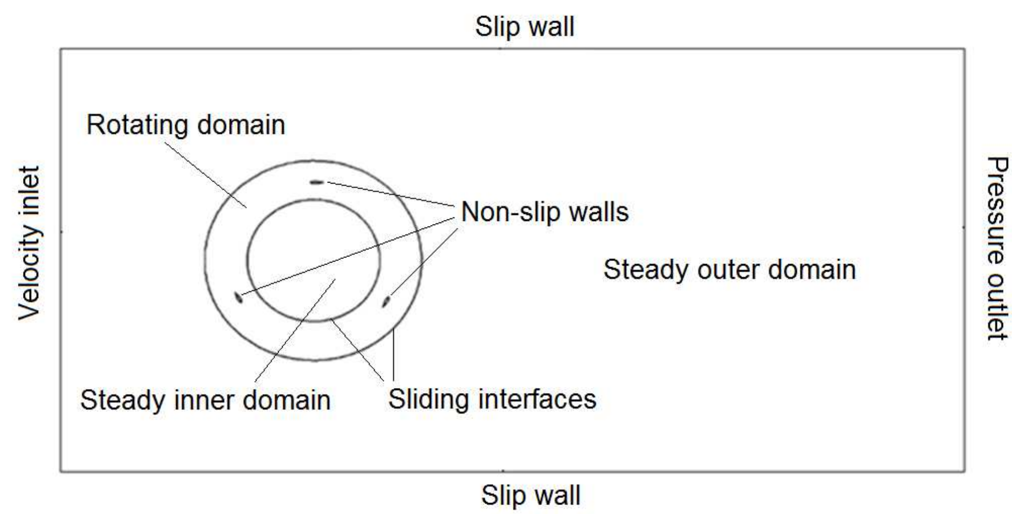

Fig. 2. Geometry and boundary conditions employed for the simulated three-bladed CFWT described in [15].

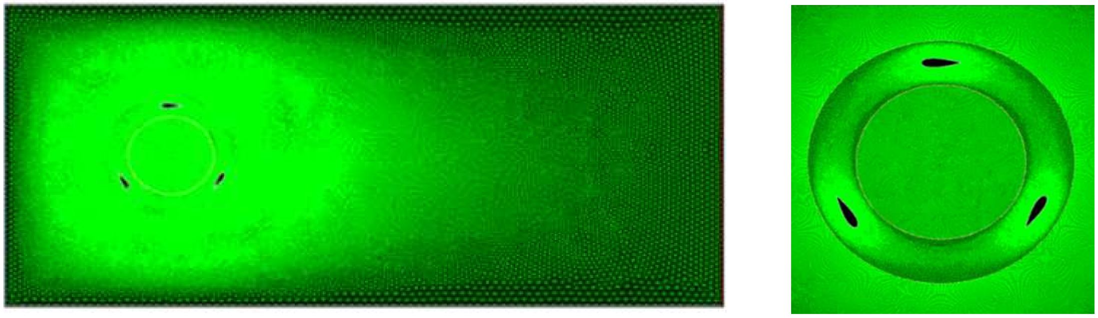

Fig. 3. Details of the generated grid. Right: detail of the grid in the rotating ring containing the profiles.

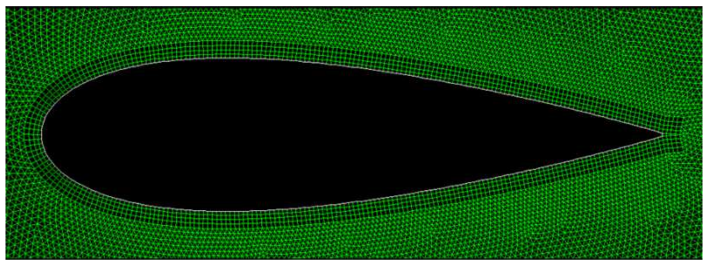

Fig. 4. Detail of the grid near the profile surface showing the prisms layer.

In the case of the CFWT, the computational domain consists of a rotating zone (the rotor in a ring-like domain) and a steady zone. The last one includes the water environment outside and inside of the ring-like domain (see Fig. 2).

The computational domain was meshed using a non-structured grid generated with the software GAMBIT (Fig. 3). The mesh closest to the profiles must be refined enough to be able to describe with sufficient precision the boundary layer flow. To this end, the created mesh had an O-grid topology based on quads and it is shown in Fig. 4. Outside of this prisms layer, a non-structured grid based on triangles was chosen, keeping an aspect ratio similar to that of the quads [7].

The steady domain was also discretized with a non-structured grid based on triangles (Fig. 3). As it can be observed, the grid node density is higher near the blades than in the rest of the domain. Moreover, due to the complexity of the flow in the turbine wake, also the grid node density is higher downstream than upstream the CFWT.

Obviously, the most interesting zone for the simulation is the ring-like domain, because is here where the flow interacts with the blades, which is responsible for the turbine performance. Again, in this region the grid node density is higher than in the steady domain.

4 Numerical simulation methodology

Numerical simulations of the straight-bladed CFWT were carried out using the software ANSYS-CFD, based on the finite volume method. The present two-dimensional simulations were carried out with Fluent due its flexibility to deal with complex geometries.

In the unsteady simulation a transient rotor stator model was employed to capture the change of the flow field at a particular time. A moving mesh technique was applied in order to rotate the turbine blades at a constant rotational speed and, at first instance, the Shear Stress Transport (SST) k-ω turbulence model was used to model the turbulent features of the flow. This method is a combination of the k-ε and k-ω models (Menter, 1994) [31]: it uses the k-ω model near the wall and switches to a function of the k-ε model when moving away from the wall closer to the upper limit of the boundary layer. The SST k-ω model has been shown to perform better for flows with strong adverse pressure gradients such as those appearing in the CFWT flow configuration, being able to describe the generation of specific vortices at the leading and trailing edges respectively. The governing equations of the SST k-ω turbulence model are given in Menter [31] and will not be repeated here. In a later section, the influence of the turbulence model on the predicted turbine performance will be addressed.

The effectiveness of physical transport within the solver depends not only on the turbulence model but also on the discretization scheme. The diffusive term in the equations is discretized using second order centered differences as usual. However, for the advection term a second order upwind scheme is utilized. The pressure-velocity coupling algorithm chosen has been the transient Semi-Implicit Method for Pressure-Linked Equations (SIMPLE). Finally, the time integration is performed by a second order implicit scheme to obtain a good resolution in time.

Typically, the simulation starts with the computation of the steady flow around a fixed position of the turbine blades. From this initial condition, the transient simulation begins, firstly with first order schemes to ease convergence. Once that the total torque on the turbine has reached a quasi-periodic regime, after three or four complete rotor revolutions, the discretization schemes are switched to second order. Finally, the simulation runs during a sufficient number or rotor revolutions (usually six) in the quasi-periodic regime to extract an average value for the torque, which is used to estimate the turbine performance.

5 Grid verification and validation

The verification process of the CFD simulation implies to perform calculations in different grids varying the number of elements, for evaluating convergence of most relevant variables. In this case the non-dimensional torque transferred from fluid to blades, C_m, has been chosen. The number of grid nodes were: coarse mesh, 60,558; medium mesh, 157,130; and fine mesh, 297,302. Results of validation in three different grids for average torque coefficient were: coarse, 0.1200; medium, 0.1399; and fine, 0.14352. Fig. 5 presents the mean value of power coefficient (equal to the product of torque coefficient C_m and tip speed ratio λ) along a complete revolution, at TSR = 1.745, for the three grids as function of the mesh relative size. It is defined as $\Delta x/\Delta x_{fine}$ (Δx is the characteristic size of the cell in the considered mesh), where value 1 corresponds to the finest mesh considered. In Fig. 5, also the Richardson extrapolation, representing the asymptotic value of average power coefficient in the limit of number of nodes tending to infinity, is shown. According to the standard analysis of mesh independence verification [32], the intermediate size mesh was selected, as the grid density is already in the asymptotic range of convergence, as a compromise between precision and computational cost.

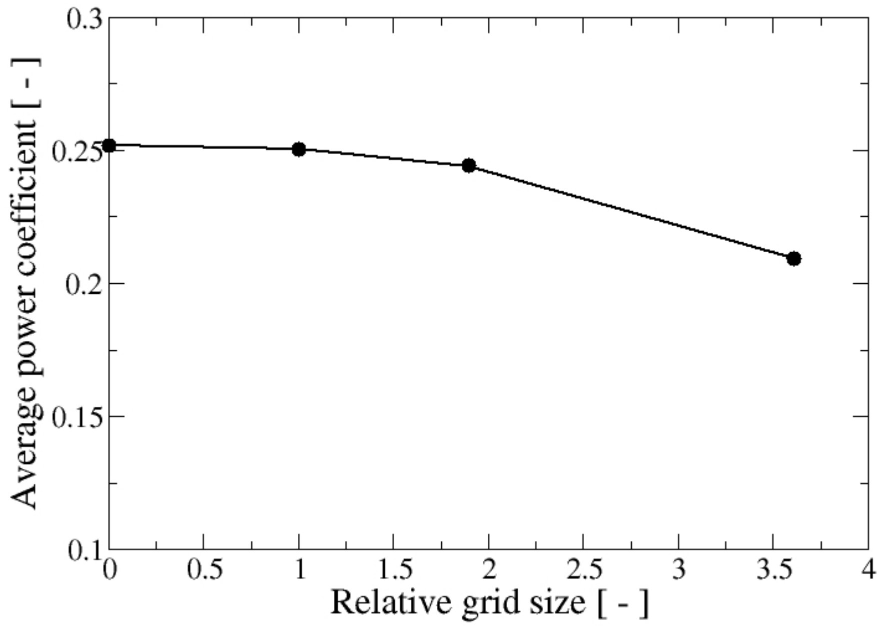

Fig. 5. Power coefficient at λ = 1.745 in the grid convergence study

Moreover, a temporal verification study was performed for the medium grid. As a result, a time step of Δt = 5 ms was adopted, which is the same employed in [15]. Fig. 6 shows the torque coefficient obtained with different time steps along a complete revolution of the blades for a tip speed ratio of λ = 1.745.

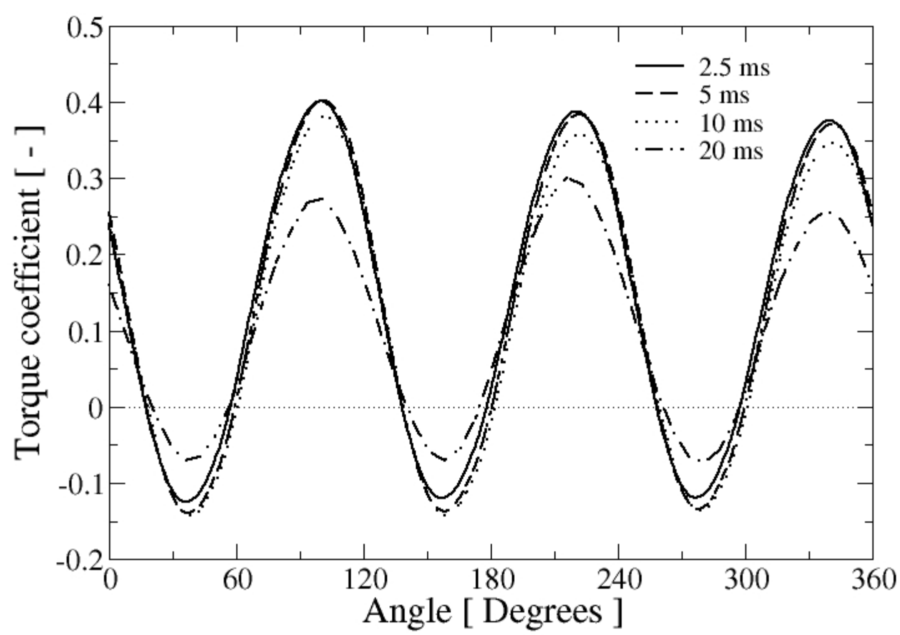

Fig. 6. Torque coefficient for different time steps in the medium grid, λ = 1.745

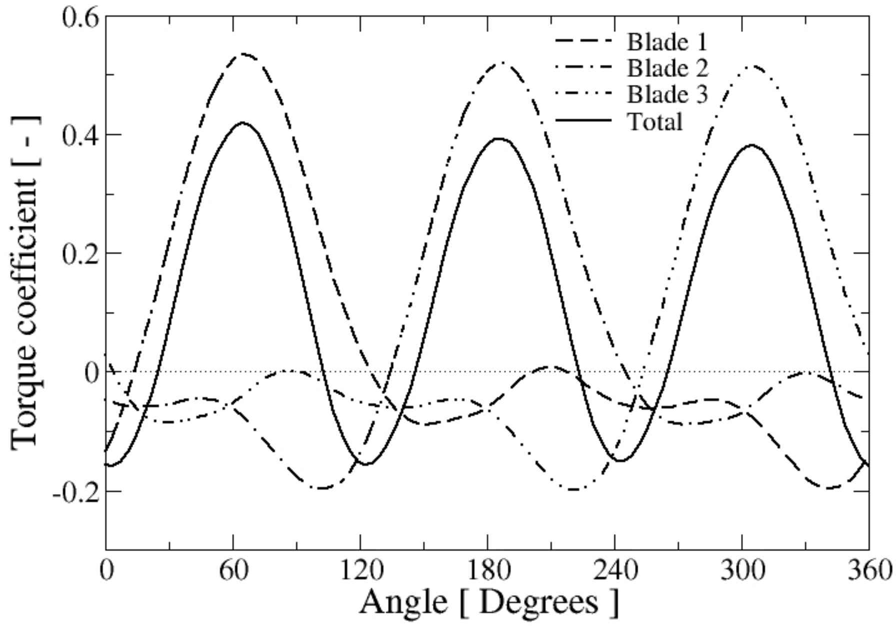

Fig. 7. Generation of torque coefficient by each blade in a revolution

After a time of around 6 s, C_m reached a quasi-periodic regime after initial transient. Both maxima and minima of C_m for each blade have higher absolute value than total C_m due to existence of cancellations and compensations of torque among blades, resulting in a total maximum C_m lower than that experienced by a single blade. The flow field around the turbine is quite complex because, as the blades rotate, high and low velocity zones appear, leading to a detachment of the boundary layer in certain angular positions. Moreover, the flow behind the CFWT is characterized by low velocities which imply a smaller contribution to the total torque than in the upstream region. As a result, in a turn, each blade produces a positive C_m in about a third of revolution, whereas in other two thirds, C_m is slightly negative. After averaging the three coefficients generated by blades, a nearly sinusoidal curve is obtained with three positive maxima at each turn (Fig. 7) and three negative minima, meaning that during a revolution there are periods of time where turbine produces torque on fluid. The number of maxima at each turn equals number of blades of turbine.

The plot of average power coefficient versus tip speed ratio λ (Fig. 8) shows positive values up to λ close to 2.1, meaning that the fluid is providing torque to the turbine. Beyond $\lambda = 2.1$ the power coefficient is negative which indicates that the turbine, rotating at constant angular speed, delivers energy to the fluid. This situation appears because a high tip speed ratio implies a high turbine angular speed and, in such case, the kinetic energy contained in the flow is not enough to deliver torque to the CFWT and to make it rotate with the same angular velocity. On the other hand, the curve $C_P(\lambda)$ presents a maximum around $\lambda = 1.55$ and decreases for lower values of the tip speed ratio. This behavior is due to the fact that, for low values of λ, the flow around the blades is separated implying low lift and high drag. As a result the transferred energy from the fluid to the turbine decreases.

It can be observed in Fig. 8 that the maximum power coefficient predicted by CFD is around 36% at λ = 1.55. Similar C_P curves are found in other CFWT [6, 14]. Unfortunately, Dai and Lam (2009) [15] only provide data for a single point with λ = 1.745, instead of the full $C_p(\lambda)$ curve, which is also shown in Fig. 8.

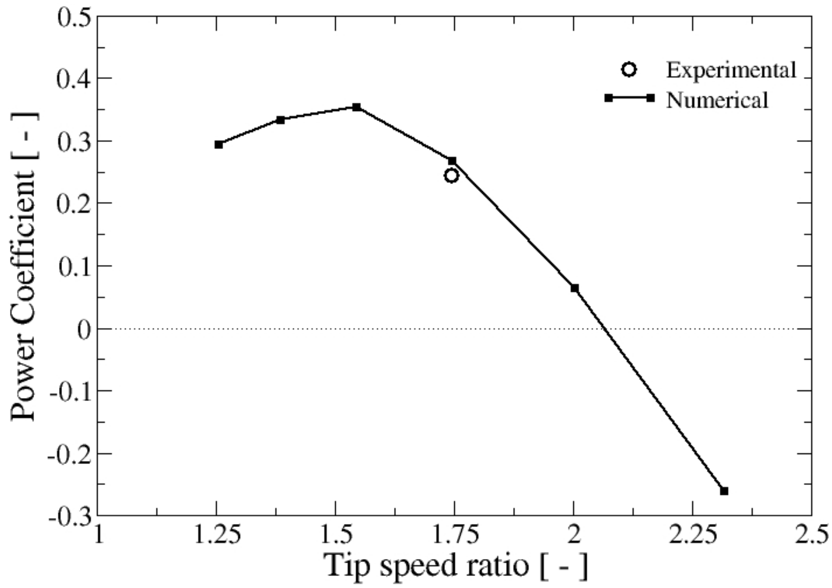

Fig. 8. Average power coefficient versus tip speed ratio λ.

Finally, as a comment, the present computed power coefficient is higher than the experimental value, a fact already found in other two-dimensional simulations [13,16].

6 Sensitivity of results to turbulence model

To study the sensitivity of results regarding the employed turbulence model, four additional turbulence models have been tested: Reynolds Stress Model (RSM) [33], realizable k-ε [34], SST laminar-turbulent Transition and Spalart Allmaras with curvature correction (SA-RC) [35].

The Spalart-Allmaras (SA) is a one equation turbulence model extensively used in aerodynamic applications involving flow over airfoils. Its improvement involving curvature correction (SA-RC) allows the application of the standard SA to situations with strong curvature of the streamlines, and allows the computation on non-inertial rotating reference frames, such as the case considered in the present study. The realizable k-ε turbulence model, on the other hand, extends the application of the standard k-ε to flows with rotation, boundary layers with strong adverse pressure gradients, separation and recirculation. The laminar-turbulent transition SST is applicable to problems where upstream laminar boundary layers experience transition into a turbulent flow further downstream such as those that very likely develop in the CFWT blades.

In contrast to the two-equation eddy viscosity models, the Reynolds Stress Model solves independent transport equations for each component of the Reynolds Stress Tensor, avoiding the Boussinesq approximation for closing them. It is preferred when the underlying turbulence of the flow field is anisotropic, there is strong curvature of the streamlines and/or the flow is characterized by strong swirl and adverse pressure gradients.

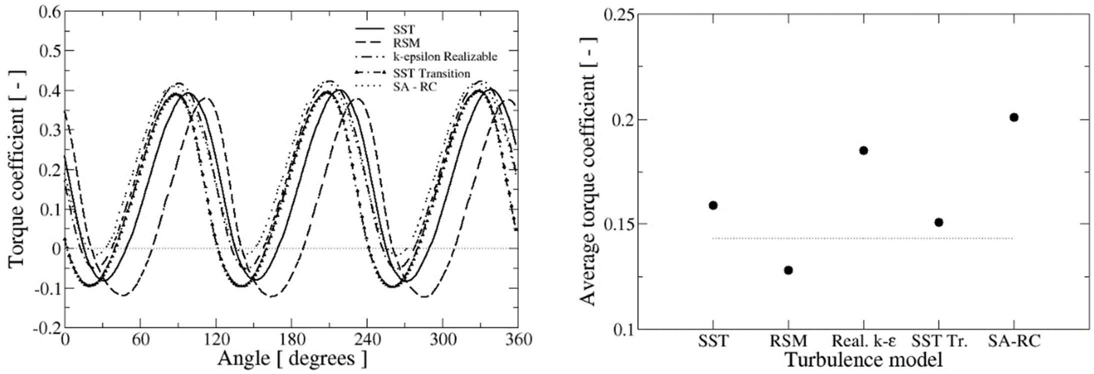

Fig. 9. Torque coefficient obtained for the different turbulence models. Left: evolution along a turn. Right: mean values obtained. The dashed line shows the expected value.

The summary of results obtained with the different turbulence models can be appreciated in Fig. 9. The left side shows the evolution of the torque coefficient along a turn for all the turbulence models tested, including the standard formulation of the SST model. In order to present the results in a more clear way, the curves for the standard SST and RSM models have been displaced towards the right, so all the curves can be appreciated in the same plot. The right side of Fig. 9, compiles the average torque coefficient values for each turbulence model, where the dotted line shows the experimental expected value. From that figure, it can be seen that the closest values to the expected value are provided by the SST and RSM models, providing the Transition SST the better results. The k-ω SST model good prediction of the expected value can be explained by the fact that it is a low-Re turbulence model that does not rely on empirical damping functions (as typical two-equation models such as the realizable k-ε model). It is well-known the advantages of this model in the prediction of boundary layers with adverse pressure gradient and separation. On the other hand, the RSM model can provide a better performance than two equation turbulence models especially in flows with sudden changes in the strain rate and with high swirl and rotation, which is the case of the simulation of vertical axis turbines. The fact that the airfoil Reynolds number is changing in time can explain the observation that the transition SST model provided the numerical result that is closest to the expected value. Several phenomena that are actually happening in the boundary layer such as laminar boundary layer, transition to turbulence, laminar separation, flow reattachment and turbulent separation can be captured by the transition model. Typically, a fully turbulent model cannot predict or capture these phenomena, even though the production of turbulent kinetic energy can be controlled with a damping function. In the case of the SST transition model, two extra equations control the laminar-turbulence transition: one for the intermittency and the other for the transition momentum thickness Reynolds number. Figure 10 shows the intermittency contour close to a blade located at $\theta = 0°$, it is observed that for this specific position of the blade the boundary layer in both, upper and lower sides of the blade have a significant portion of laminar boundary layer (intermittency lower than 1). Figure 11 shows the skin friction coefficient (C_f) distribution along the airfoil surface for the same position ($\theta = 0°$), it is clear that in the case of the SST k-ω model the prediction of C_f is higher than for the SST transition model. It is also appreciated that for the transition model the boundary layer has a laminar, transition and turbulent regions so that the predicted force is different for the two models, it is actually 3N lower for the SST transition model in comparison to a fully turbulent model as SST k-ω.

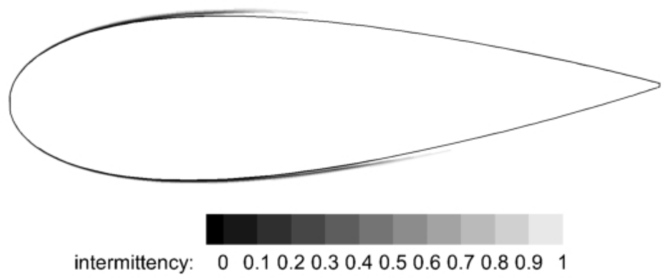

Fig. 10. Intermittency function contour values for a blade at position θ = 0°. Dark colors indicate laminar boundary layer development from the leading edge.

A point to be marked is that all the two-equation models provide values for the torque coefficient above the expected one, but the RSM provides in this situation a lower value. In that case, two different inlet conditions were tested for the Reynolds Stress components: the first one considered isotropic normal stresses, while in the second the streamwise normal stresses $\overline{\boldsymbol{u}'\boldsymbol{u}'}$ were higher than the transversal normal stresses with a turbulence intensity of 10% in the flow direction. Although not shown, the final results did not reflect any significant influence of this inlet boundary condition.

Moreover, Fig. 9 (right) clearly shows that the poorest performance is that of the SA-RC model, even when this model includes the curvature correction. Therefore, this model is unable to describe correctly the turbine performance. The realizable k-ε model is also not able to provide close enough results for the average torque coefficient, in spite that it includes specific terms to handle flows with curvature and significant adverse pressure gradients.

Table 1 presents the computational cost (in minutes) needed by the turbine to perform one turn when the flow is already established. Computations were performed on a workstation Dell Precision T5500 with a quadcore Intel Xeon 5600 processor. At each time step a maximum of 40 iterations is allowed. As expected the RSM is the most expensive, needing approximately 30% more iterations than the others due to the need of solving five extra differential equations. Unexpectedly, apart from the loss of precision, the SA-RC model is as expensive as a two-equation model. This finding discourages its use as one of the main advantages of the SA model is its low computational cost. The production term in the SA equation (normally treated as a source) increases in the SA-RC model so that the convergence of the SA equation takes more time per iteration that the SA model.

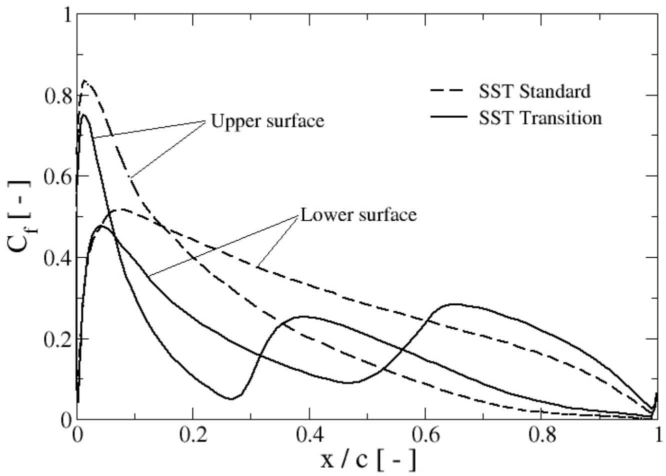

Fig. 11. Skin friction coefficient variation along the profile chord for the SST turbulence models considered.

Table 1. Computation time for the different turbulence models.

Turbulence model	Iterations 1 turn	Time [min]
RSM	8000	33
SST Standard	6436	21
k-ε Realizable	6500	20
SST Transition	6231	26
SA-RC	6299	24

7 Two-dimensional optimization parametric studies

For the parametric two-dimensional study, the same characteristics of the case 3S2R1 of reference [15] were used and kept constant except for the airfoil geometry which changes between computational experiments. In this case, the commercial software Gridgen was used to generate the mesh and to ensure that all the computational grids had the same topological details. The experimental design (a factorial 3^2) for the parametric study consists in developing a series of tests in which the geometry of the airfoil is changed to determine its influence on the performance of the turbine. The airfoils used here are NACA 4-digit series, which are characterized by its camber and thickness [36]. These two geometric variables of the airfoil profile were used as factors, each one with 3 levels as shown in Table 2. In total 9 different meshes were generated for each computational experiment proposed for the parametric study.

Table 2. Factors and levels for the design

Factor	Level		
	Low	**Medium**	**High**
Thickness (as % of c)	6	12	15
Camber	00XX	24XX	44XX

A Gridgen script written in Glyph language was created in order to ensure that the mesh generated is similar for all the computational experiments. The mesh generation starts by defining the airfoil profile with the maximum thickness (t) as a fraction of the chord, the maximum camber (m) also as a fraction of the chord and the location of the maximum camber (p) as a tenth of the chord. With these parameters the lower and upper surfaces of the airfoil are created and divided in a fixed number of elements. Then, a hyperbolic mesh is generated from the profile in order to define the boundary layer region. The script allows controlling the size of the first element, growth rate, the size of the boundary layer region and the number of cells on it. The size of the first element and the growth rate are important to capture the physics of the flow close to the airfoil (Fig. 12 left). Depending on the radius and the number of blades of the turbine, the airfoil and the boundary layer mesh is copied and pasted in the correct location. Then the rotating domain and the steady inner domain are created and meshed with triangular elements. The growth rate between the boundary layer region and the rotating domain is also specified in order to achieve a smooth transition between the structured and unstructured meshes (Fig. 12 right). Finally, the steady outer domain is generated and meshed with triangular elements. The growth rate in the free stream direction can be also controlled and specified. The different parameters in the mesh generation were fixed and their values were achieved after a grid convergence study.

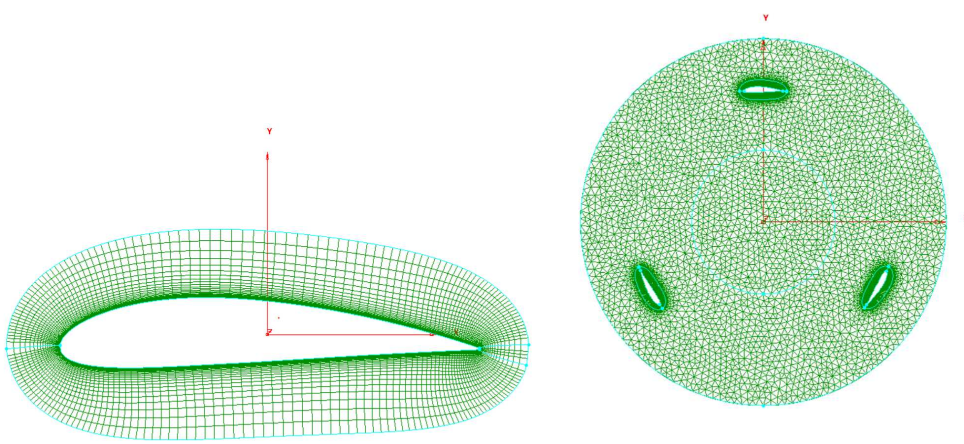

Fig. 12. Generation of the hyperbolic mesh around the profile (left) and mesh in the inner domain (right).

Integral results based on moment, tangential force and normal force coefficients were statistically analyzed using the commercial software Minitab. The moment coefficient (C_m) was computed in the turbine shaft showing a similar behavior and magnitude to Fig. 7. The influence of thickness and camber on the average C_m for each airfoil profile is shown in Fig. 13 (left). It is clear that the thickness is the most important parameter in the turbine performance at this point of operation (λ = 1.745). As the airfoil becomes thicker, better performance is achieved. However, C_m does not improve significantly for airfoils thicker than 15% of its chord. In order to confirm the observed influence of the thickness an Analysis Of Variance (ANOVA) [37] was performed, in which the p-value found for the thickness is below 0.05 while for the camber was 0.193. Camber seems to have an important influence when thin airfoils are used, but it does not make a difference as the airfoil thickness increases. Fig. 13 (right) shows the evolution of C_m for the thicker airfoils with different camber, in which it is observed that there is no significant difference in the averaged C_m. Nevertheless, NACA4415 shows a smaller negative C_m region which is desirable for smooth turbine operation.

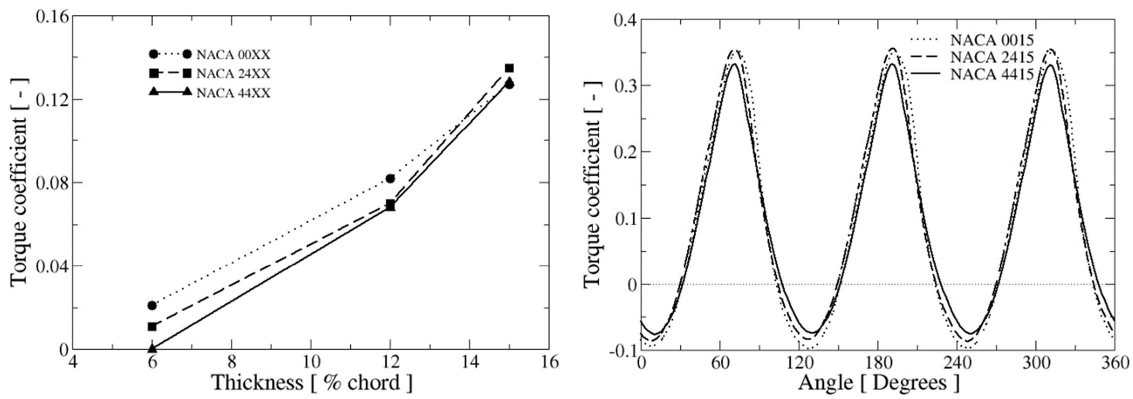

Fig. 13. Left: Influence of symmetry / asymmetry and thickness on C_m. Right: C_m comparison for different airfoil camber along a complete revolution.

The tangential force coefficient (C_t) has also a cyclic behavior related to C_m. Since the behavior of C_t is similar for all the blades, only one blade whose motion starts at $\theta = 0°$ will be analyzed. Fig. 14 (left) shows the evolution of C_t for one blade with different camber. It is clear that NACA0015 airfoil presents the deepest minimum which is a desired condition since the performance increases, but it is also observed that between 210° and 40° this airfoil does not produce torque. As the camber increases the contribution of the airfoil in the total torque improves (between 250° and 360°). This observation supports the argument that camber could improve a smooth turbine operation, since during one rotation of the turbine at least one of the blades is always producing negative tangential force. Average values of C_t for one blade are computed and compared (Fig. 14 right), it is clear that the thickness is the most important factor that influences the tangential force. It is also observed that the camber drives the averaged tangential force into more negative values, in particular for thicker airfoils. In order to confirm the observed influence of the thickness an ANOVA test was performed, in which the p-value found for the thickness is below 0.05 while for the camber was 0.41.

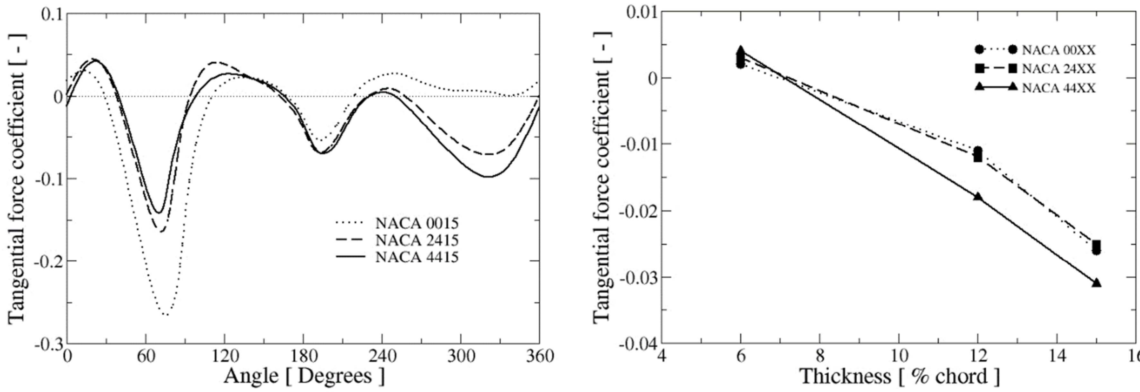

Fig. 14. Left: C_t comparison for one blade for three different camber. Right: Influence of symmetry / asymmetry and thickness on C_t.

The normal force coefficient (C_n) presents a cyclic behavior too. Similar to the analysis performed to C_t, only one blade whose motion starts at $\theta = 0°$ will be studied. Fig. 15 (left) shows the evolution of C_t for one blade with different camber. It is observed that the curve is shifted towards zero as the camber increases. The influence of the airfoil thickness and camber is shown in Fig. 15 (right), in this case the camber is the factor that primary influences the normal force. This observation is confirmed with an ANOVA test, in which the p-value found for the camber is below 0.05 while for the thickness was 0.47. The average normal force is related to the resultant force on the turbine shaft. From this analysis, it is concluded that a cambered profile could improve the resistance of a specific turbine design to fatigue failure.

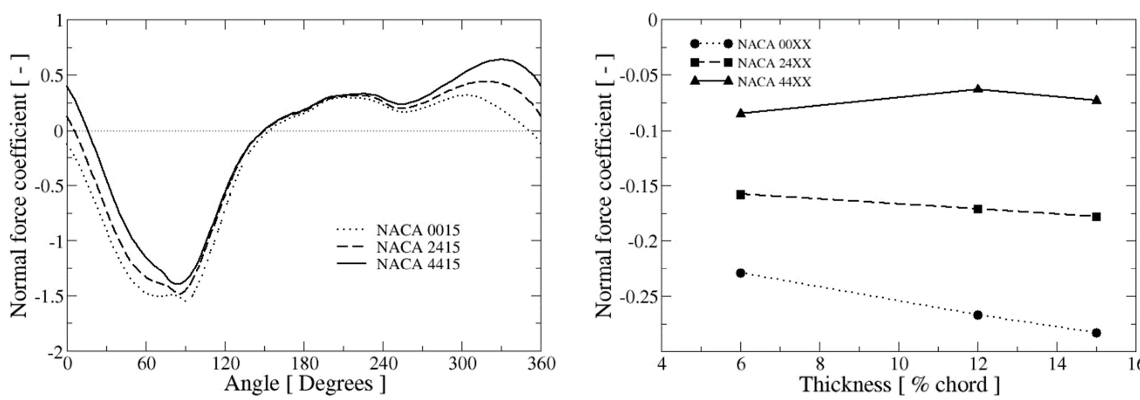

Fig. 15. Left: C_n comparison for one blade for three different cambers. Right: Influence of symmetry / asymmetry and thickness on C_n.

Fig. 16 illustrates the evolution of the vorticity field (magnitude) during one cycle of the turbine with the NACA4415 airfoil. In that figure, the water flow progresses from left to right and transition from one image to next corresponds to a change of 15^{o} in the airfoil position. When the cycle starts ($\theta = 0°$) a vortex is visible in the trailing edge of the blade. Also at this position the blade experiences the interference with the wake of the former blade as it can be seen in Fig. 16 a). The vortex stays attached to the trailing edge up to $\theta =$ 60°, where a vortex layer starts to grow in the lower surface of the blade, corresponding to the wake, consisting of a recirculation bubble, generated on the rear side of the profile which starts to be faced to the main flow direction (Fig. 16 e). This observation is consistent with the increase in C_n since the lower surface of the airfoil is exposed to a very low pressure while the upper surface of the airfoil has a high pressure. Such recirculation bubble grows continously up to θ = 120° (Fig. 16 a) where two vortical regions can be appreciated, one larger in the upper surface and other smaller near the trailing edge. At θ = 135° (Fig. 16 b) the recirculation bubble is about to detach from the airfoil leading edge and the vortex attached to the trailing edge starts to be convected downstream by the main flow. At θ = 135° (Fig. 16 c), the large recirculation bubble is detached from the profile and a new leading edge vortex starts to be formed. However, the detached vortex, convected by the free stream flow, stays near of the blade, with decreasing intensity, as it progresses up to θ = 180° (Fig. 16 e). Figs. 16 f) to h) show clearly how such vortex interacts with the blade. Some authors have pointed out that this vortex dynamics prevents the turbine from suffering a drop of efficiency at this point as a local high negative value of tangential force is attained along this part of the blade path (see Fig. 14 left). At the same time the leading edge vortex starts to be developed in the upper surface of the airfoil forming a recirculation bubble in this region and the small trailing edge vortex is convected by the main flow being displaced from the lower to the upper surface of the airfoil. At θ = 225° the collision of the formerly detached vortex with the blade is clearly observed (Fig. 16 h). At θ = 255° (Fig. 16 b) the elongated leading and trailing edge vortices interact forming a wide wake in the upper surface of the blade, creating strong pressure drag. Such wake is convected downstream as the profile progresses (Figs. 16 c) to e) while the region of high vorticity becomes thinner, corresponding to the progressive alignment of the profile with the main flow. At the end of the cycle, a strong wake is formed which is convected downstream. Moreover, the airfoil interacts with the wake generated by the previous profile (low pressure region) (Figs. 16 f) to h).

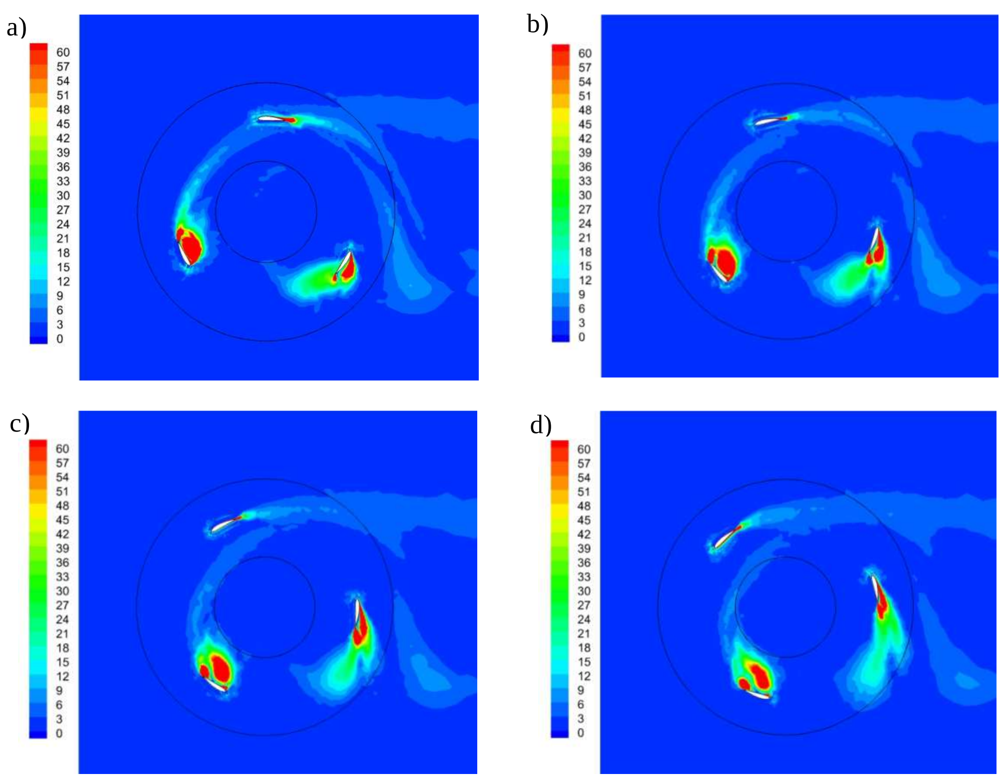

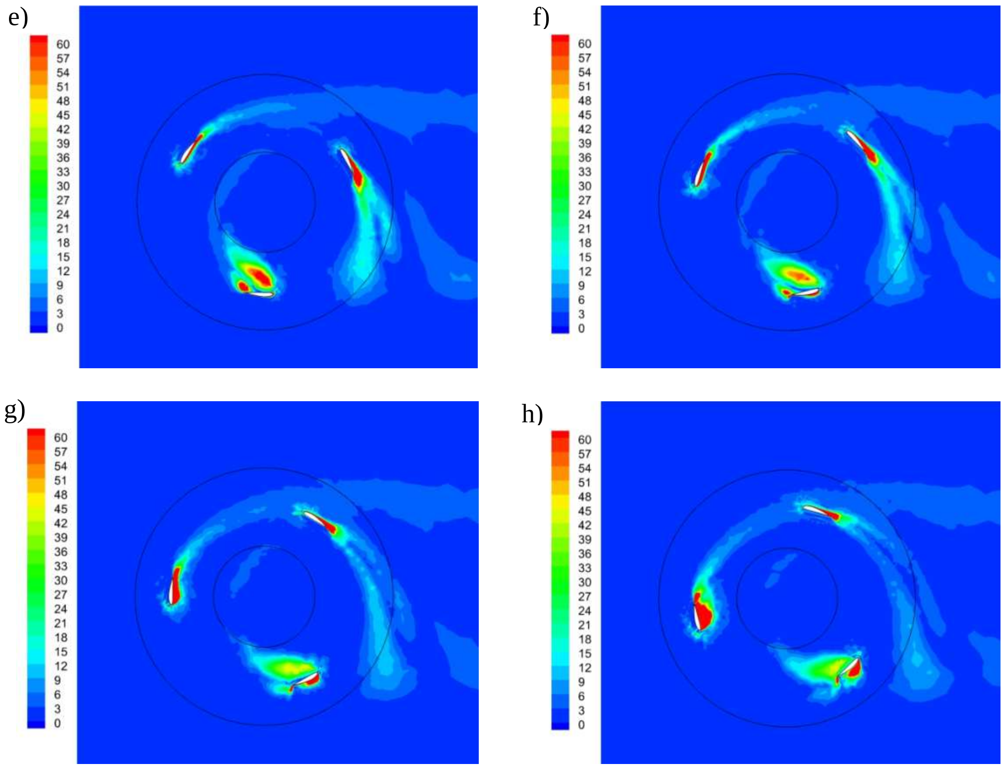

Fig. 16. Vorticity field (magnitude in 1/s) evolution in one cycle. From one image to the next, each airfoil experience a change of 15^{o} in its angular position.

8 Blockage ratio influence on numerical results

Next the influence of the blockage ratio on the predicted turbine performance is assessed. Regarding the basic case, described in section 3, with a height/length (h/l) relation of 5:8, three additional cases where considered: h/l = 15:64, 5:16, 15:16.

The obtained results for the torque, tangential and normal force coefficients are presented in Figs. 17 and 18. For the analyzed h/l relations an asymptotic trend is observed as it increases, i.e. the influence of the blockage diminishes, for the three coefficients (torque, tangential and normal force). Moreover, also the increase of turbine performance can be noticed as the blockage ratio augments, which is an interesting result for ducted turbines [14]. The strongest impact is on the normal force, where the change among the studied h/l relations is more than 20%. This observation is interesting from the turbine design point of view, because an increase in the blockage ratio also implies higher loads on the blades and turbine axis. Also, for a relation of $h/l > 0.6$ (around a blockage ratio of 20%) the results are very approximately independent of it, representing free flow conditions.

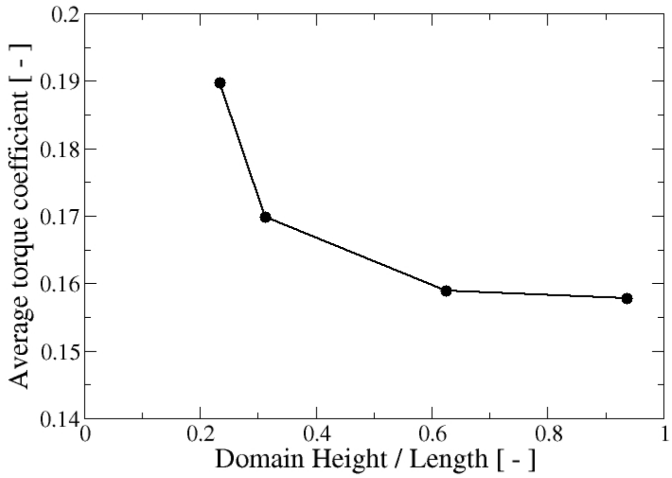

Fig. 17. Results of torque coefficient for different relations *h*/*l*.

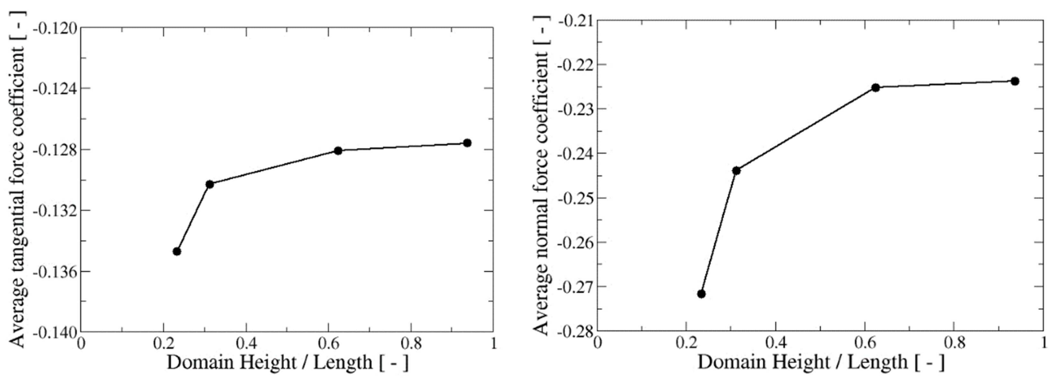

Fig. 18. Results of tangential (left) and normal (right) force coefficients for different relations *h*/*l*.

9 Sensitivity of results to trailing edge geometry

In order to study the influence of the trailing edge (TE) geometry in the predicted hydrodynamic performance of the turbine, three different TE geometries were simulated. The easiest way to model the TE is by truncating the airfoil profile using a straight line (see Fig. 19 left). The other two geometries tested were a sharp and a rounded TE, as shown in Fig. 19, center and right, respectively. These geometries were tested for the NACA4415 airfoil.

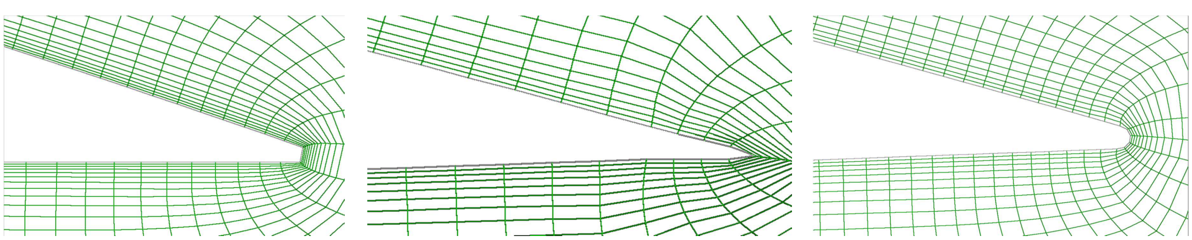

Fig. 19. Configuration of trailing edges considered: left, truncated; center, sharp; right, rounded.

As shown in Fig. 20, the averaged torque coefficient increases when the trailing edge geometry has a smooth transition (rounded TE), which responds to an increase in the absolute value of the maximum of the tangential force coefficient. Although not shown, the normal force coefficient does not present a significant dependence on the different tested trailing edge geometries. Therefore, it can be stated that for the design of the profiles used in studies, it is important to model the trailing edge with smooth transition as possible; this leads to better results in torque coefficient, that increase the efficiency of the turbine. A rounded TE provides a smoother pressure distribution between the lower and the upper side of the blade, which also helps in a smooth evolution and separation of the wake. It was observed that a rounded edge gives positive lift on the upper surface near the trailing edge, while a sharp edge has negative lift, slightly changing the Kutta condition. It is generally considered that truncated or rounded TE are easier to manufacture in comparison to sharp TE; however, they are not commonly use in pure aerodynamic applications although they have been investigated for wind turbine applications [38].

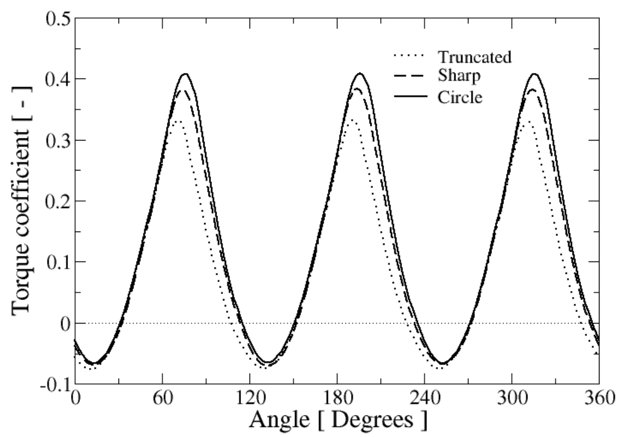

Fig. 20. Torque coefficient for the different types of TE considered.

10 Comparison with preliminary 3D computations

In order to provide an estimation of three dimensional effects on the predicted performance of the CFWT, preliminary results obtained from a 3D computation are presented. As in the two-dimensional case neither the shaft or supporting arms have been included in the simulation. Also, a symmetry plane was employed at rotor mid-span to reduce computational requirements and the sliding mesh strategy was used to model the unsteady flow around the turbine. The chosen turbulence model was SST, the same as in the 2D case, combined with second order discretization schemes in the space as well as in time. Finally, the employed time step was also 5 ms. The fairly coarse employed unstructured grid comprises around two-million elements.

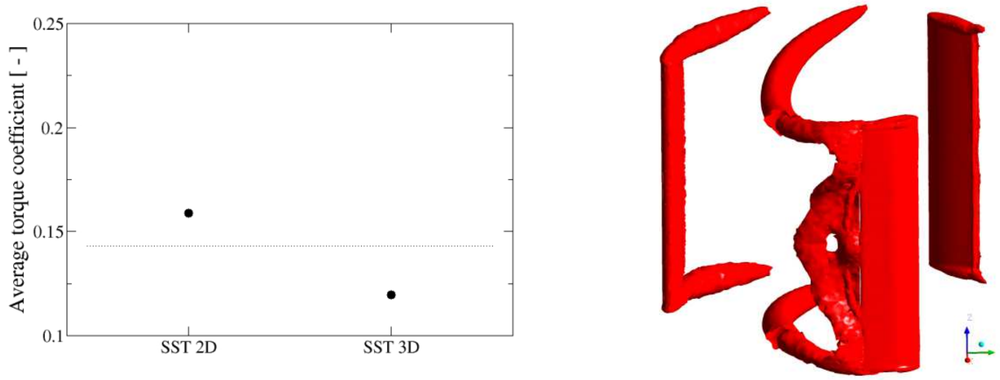

Fig. 21. Left: Predicted torque coefficient in the 2D and 3D cases compared with the experimental value (dashed line). Right: Snapshot of the trailing and bound vortices on the 3D configuration

As it can be clearly observed from Fig. 21 (left) the predicted average torque coefficient is lower than the two-dimensional prediction due to the additional loses promoted by the tip blade vortices. Such trailing tip vortices are associated with the generation of lift in three-dimensions and they are unavoidable side-effect of it. Such trailing vortices induce a downward component of the fluid velocity in the neighborhood of the blade reducing the angle of attack and creating a component of the drag, known as induced drag. Such drag component reduces the effective torque that fluid delivers to the turbine rotor and therefore, also its torque coefficient. Additionally, the predicted 3D coefficient is even below the experimental values, represented by the dashed line, which can be attributed to the fairly coarse grid employed in the 3D computation [21].

The three-dimensional simulation allows visualising clearly the shape and topology of the trailing vortices at certain moment of turbine rotation. In Fig. 21 (right), the main flow is aligned with the positive y-axis and the vortices are illustrated as an isosurface of vorticity intensity of 40 s^{-1}. In such figure, it can be appreciated the geometry of the trailing vortices, attached to the blade tip, which are curved in the direction of the main flow and eventually are convected downstream. Also the blade bound vortex shape can be observed in the same figure; near of the symmetry plane the vorticity isosurface is separated from the trailing edge but near the tip it is still attached to the blade. The vortex bending towards the inner ring-like domain can also be appreciated and it is due to the non-linear self-interaction of the vortex. This fact can be explained as follows: the wake downstream the blade consists of a finite-thickness vortex sheet that under self-induction evolves into a hairpin vortex (which is a characteristic structure present in turbulent shear flows) with high values of shear Reynolds stresses [39].

Currently, the authors are performing more refined three-dimensional computations of CFWT, in order to quantitatively investigate the effects of tip vortices presence and detachment on CFWT power coefficient prediction.

Conclusions

A study of the unsteady flow around a CFWT with the commercial code ANSYS-CFD has been carried out using a transient rotor-stator approximation with a sliding mesh technique in turbulent flow. Simulation results are in agreement with reported experiments in a laboratory CFWT [15]. Moreover, the average power coefficient versus tip speed ratio curve has been constructed for the considered turbine.

Regarding the sensitivity of results on the turbulence model, the present findings discourage the use of the Spalart-Allmaras model (even with curvature correction) and favor the use of the SST type of turbulence models as they represent a compromise between precision and computational time.

In the optimization study, the factorial 3^2 experimental design performed in the present analysis demonstrated the influence of the thickness parameter in the moment and tangential force coefficients. Both C_m and C_t asymptotically increase as the thickness of the airfoil increases. For airfoil profiles with thickness greater than 15% of the chord length, the increase in C_m and C_t is not significant. The results of the parametric study also demonstrate the influence of the camber on the normal force coefficient. Even though performance is the primary consideration for a vertical-axis turbine, the cyclic bending loads on the turbine shaft are also important for design. Based on the numerical results, a cambered airfoil decreases the average load on the shaft and could improve the resistance of a specific turbine design to fatigue failure.

The numerical results about the influence of the blockage ratio have demonstrated that the domain size must be at least h/l = 5:8 (or 20% maximum blockage ratio) to simulate the behavior of a turbine in free flow. A higher blockage ratio implies an increase of the predicted turbine performance, which is the case in ducted turbines, but also a significant increase on blade and turbine shaft loads. Additionally, the predicted turbine performance improves when smooth trailing edge geometry of the airfoils is employed. Finally, a comparison of predicted torque coefficient between 2D and preliminary 3D simulation was carried out; as a result, the corresponding values for the three-dimensional case are below the two-dimensional ones due to the generation of induced drag by the detached vortices from the blade tip. The geometry and shape of trailing and bound vortices have also been illustrated by the results of the three-dimensional computation.

All together, the results obtained in this work demonstrate that CFD can effectively assist the processes of design, evaluation and optimization of hydrodynamic performance of cross flow water turbines.

Acknowledgement

The financial support of the Dirección de Investigaciones y Desarrollo Tecnológico of Universidad Autónoma de Occidente is gratefully acknowledged. This work was partially sponsored by the Young Researchers program from the Colombian administrative department of science, technology and innovation (Colciencias) and also by Vicerrectoria de Investigaciones of Universidad de los Andes.

References

[1] Black and Veatch Consulting Ltd. UK: Europe and global tidal stream energy resource assessment. Peer review issue 107799/D/2100/05/1, Carbon Trust, London, September 2004.

[2] Kerr, D.: Marine Energy. Phil. Trans. R. Soc. A, **365**, 971–992 (2007).

[3] IRENA. Tidal Energy. Technology Brief. June 2014. http://www.irena.org/DocumentDownloads/Publications/Tidal_Energy_V4_WEB.pdf

[4] Dabiri, J.: Potential order-of-magnitude enhancement of wind farm power density via counter-rotating vertical-axis wind turbine arrays. Journal of Renewable and Sustainable Energy **3**, 043104 (2011).

[5] Duraisamy, K., Lakshminarayan, V.: Flow physics and performance of vertical axis wind turbine arrays. Proc. 32nd AIAA Applied Aerodynamics Conference, 16-20 June 2014, Atlanta (USA). Paper AIAA 2014-3139 (2014).

[6] Coiro, D.P., De Marco, A., Nicolosi, F., Melone, S., Montella, F.: Dynamic Behaviour of the Patented Kobold Tidal Current Turbine: Numerical and Experimental Aspects. Acta Polytechnica Czech Technical University in Prague **45**, 77 – 84 (2005).

[7] Laín, S., García, M., Quintero, B., Orrego, S.: CFD numerical simulation of Francis turbines. Revista Facultad de Ingeniería Universidad de Antioquia **51**, 21 – 33 (2010).

[8] Laín, S., Aliod, R.: Study of the Eulerian dispersed phase equations in non-uniform turbulent two-phase flows: Discussion and comparison with experiments. Int. J. Heat Fluid Flow, **21**, 374 – 380 (2000).

[9] Göz, M.F., Laín, S., Sommerfeld M.: Study of the numerical instabilities in Lagrangian tracking of bubbles and particles in two-phase flow. Computers and Chemical Engineering, **28**, 2727 – 2733 (2004).

[10] Ferreira, C.J.S.: The near wake of the VAWT. 2D and 3D views of the VAWT aerodynamics. Ph.D. Thesis, Delft University of Technology (2009).

[11] Maître, T. Achard, J.L. Guitet, L. Ploesteanu, C.: Marine turbine development: numerical and experimental investigations. Scientific Bulletion of Timisoara Politechnic University **50**, 59 – 66 (2005).

[12] Laneville, A., Vittecoq, P.: Dynamic Stall: The Case of the Vertical Axis Wind Turbine. Journal of Solar Energy Engineering **108**, 140 – 145 (1986).

[13] Howell, R., Qin, N., Edwards, J., Durrani, N.: Wind tunnel and numerical study of a small vertical axis wind turbine. Renewable Energy **35**, 412 – 422 (2010).

[14] Nabavi, Y.: Numerical study of the duct shape effect on the performance of a ducted vertical axis tidal turbine. M.Sc. Thesis. British Columbia University (2008).

[15] Dai, Y. M., Lam, W. Numerical study of straight-bladed Darrieus-type tidal turbine. ICE-Energy **162**, 67 – 76 (2009).

[16] Amet, E., Maître, T., Pellone, C., Achard, J.L.: 2D numerical simulations of blade-vortex interaction in a Darrieus turbine. J. Fluids Eng. **131**, 111103 (2009).

[17] Brochier, G., Fraunie, P., Beguier, C., Paraschivoiu, I.: Water channel experiments of dynamic stall on Darrieus wind turbine blades. Journal of Propulsion and Power **2**, n 5, 445 – 449 (1986).

[18] Fujisawa, N., Shibuya, S.: Observations of Dynamic Stall on Darrieus Wind Turbine Blades. J. Wind Eng. Ind. Aerodynamics **89**, 201 – 214 (2001).

[19] Li, Y., Calisal, S.M.; Three-dimensional effects and arm effects on modeling a vertical axis tidal current turbine. Renewable energy **35**, 2325 – 2334 (2010).

[20] Coiro, D. P., Nicolosi, F., De Marco, A., Melone, S., Montella, F.: Dynamic behavior of novel vertical axis tidal current turbine: numerical and experimental investigations. Proc. Int. Offshore and Polar Engineering Conference, 469 – 476 (2005).

[21] Maître, T., Amet, E., Pellone, C.: Modeling of the flow in a Darrieus water turbine: Wall grid refinement analysis and comparison with experiments. Renewable Energy **51**, 497 – 512 (2013).

[22] Amet, E. Simulation numérique d'une hydrolienne à axe vertical de type Darrieus. Ph.D. Thesis Institut Polytechnique de Grenoble (2009).
[23] Jin, X., Zhao, G., Gao, K., Ju, W.: Darrieus vertical axis wind turbine: Basic research methods. Renewable and Sustainable Energy Reviews **42**, 212 – 225 (2015).
[24] Song, C., Zheng, Y., Zhao, Z., Zhang, Y., Li, C., Jiang, H.: Investigation of meshing strategies and turbulence models of computational fluid dynamics simulations of vertical axis wind turbines. Journal of Renewable and Sustainable Energy **7**, 033111 (2015).
[25] Lanzafame, R., Mauro, S., Messina, M.: 2D CFD modeling of H-Darrieus wind turbines using a transition turbulence model. Proc 68^{th} conference of the Italian thermal machines engineering association, ATI2013. Energy Procedia **45**, 131 – 140 (2014).
[26] Chen, Y., Lian, Y.: Numerical investigation of vortex dynamics in an H-rotor vertical axis wind turbine. Engineering Applications of Computational Fluid Mechanics. (2015). **DOI:** 10.1080/19942060.2015.1004790.
[27] Trivellato, F., Raciti Castelli, M.: On the courant-Friedrichs-Lewy criterion of rotating grids in 2D vertical-axis wind turbine analysis. Renewable energy **62**, 53 – 62 (2014).
[28] Paillard, B., Astolfi, J., Hauville, F.: URANSE simulation of an active variable-pitch cross-flow Darrieus tidal turbine: sinusoidal pitch function investigation. International Journal of Marine Energy **11**, 9 – 26 (2015).
[29] Larsen, J., Nielsen, S., Krenk, S.: Dynamic stall model for wind turbine airfoils, Journal of Fluids and Structures **23**, 959 – 982 (2007).
[30] Nobile, R., Vahdati, M., Barlow, J., Mewburn-Crook, A.: Dynamic stall for a Vertical Axis Wind Turbine in a two-dimensional study. World Renewable Energy Congress 2011 – Sweden, 8-13 May, 2011, Lindköping (Sweden) 4225 – 4232.
[31] Menter, F. R.: Two-Equation Eddy-Viscosity Turbulence Models for Engineering Applications. *AIAA*. J. **32**, 269 – 289 (1994).
[32] Roache, P. J.: Verification and validation in computational science and engineering. Albuquerque: Hermosa Publishers (1998).
[33] Launder, B. E., Reece, G. J., Rodi, W.: Progress in the Development of a Reynolds-stress Turbulence Closure, J. Fluid Mech., **68**, 537 – 566 (1975).
[34] Shih, T.H., Liou, W.W., Shabbir, A., Zhu, J.: A New k-ε Eddy-Viscosity Model for High Reynolds Number Turbulent Flows - Model Development and Validation. Computers Fluids, **24**(3), 227 – 238 (1995).
[35] Spalart, P.R. Shur, M.: On the Sensitization of Turbulence Models to Rotation and Curvature. Aerospace, Science and Technology No 5, 297 – 302 (1997).
[36] Abbott, H., von Doenhoff, A.: Theory of wing sections: including a summary of airfoil data. Dover publications, New York (1959).
[37] Montgomery, D.: Design and Analysis of Experiments. Wiley, NewYork (2000).
[38] Baker, J. P., Mayda E. A., van Dam C. P.: Experimental Analysis of Thick Blunt Trailing-Edge Wind Turbine Airfoils. J. Sol. Energy Eng. **128**, 422 – 431 (2006).
[39] Moin, P., Leonard, A., Kim, J.: Evolution of a curved vortex filament into a vortex ring. Physics of Fluids **29**, 955 – 963 (1986).